Control of Molecular Organization and Energy Level Alignment by an Electronically Nanopatterned Boron Nitride Template

Sushobhan Joshi,[†] Felix Bischoff,[†] Ralph Koitz,[‡] David Ecija,[†] Knud Seufert,[†] Ari Paavo Seitsonen,[‡] Jürg Hutter,[‡] Katharina Diller,[†] José. I. Urgel,[†] Hermann Sachdev,[§] Johannes V. Barth,[†] and Willi Auwärter[†,*]

[†]Physik Department E20, Technische Universität München, James Franck Strasse 1, D-85748 Garching, Germany, [‡]Physikalisch-Chemisches Institut, Universität Zürich, Winterthurerstrasse 190, CH-8057 Zürich, Switzerland, and [§]Max-Planck Institut für Polymerforschung, Ackermannweg 10, D-55128 Mainz, Germany

ABSTRACT Suitable templates to steer the formation of nanostructure arrays on surfaces are indispensable in nanoscience. Recently, atomically thin sp^2-bonded layers such as graphene or boron nitride (BN) grown on metal supports have attracted considerable interest due to their potential geometric corrugation guiding the positioning of atoms, metallic clusters or molecules. Here, we demonstrate three specific functions of a geometrically smooth, but electronically corrugated, sp^2/metal interface, namely, BN/Cu(111), qualifying it as a unique nanoscale template. As functional adsorbates we employed free-base porphine (2H−P), a prototype tetrapyrrole compound, and tetracyanoquinodimethane (TCNQ), a well-known electron acceptor. (i) The electronic moirons of the BN/Cu(111) interface trap both 2H−P and TCNQ, steering self-organized growth of arrays with extended molecular assemblies. (ii) We report an effective decoupling of the trapped molecules from the underlying metal support by the BN, which allows for a direct visualization of frontier orbitals by scanning tunneling microscopy (STM). (iii) The lateral molecular positioning in the superstructured surface determines the energetic level alignment; *i.e.*, the energy of the frontier orbitals, and the electronic gap are tunable.

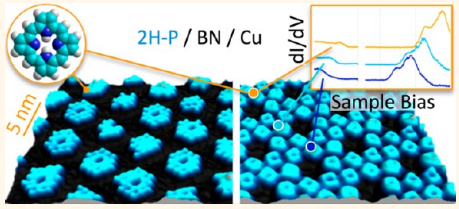

KEYWORDS: boron nitride · monolayer · moiré · scanning tunneling microscopy (STM) · scanning tunneling spectroscopy (STS) · density functional theory (DFT) · surface potential · local work function · template · porphyrin · TCNQ · confinement · self-assembly · molecular orbital

The functionalization of surfaces by molecular architectures is a promising route toward advanced materials with tailored topological, electronic, optical, magnetic or catalytic properties. Inspired by nature and supramolecular science, self-assembly protocols relying on specific interactions between programmed molecular units were successfully implemented on surfaces to achieve well-defined nanostructures.[1,2] Scanning tunneling microscopy (STM) is the method of choice to image and characterize such low-dimensional architectures with submolecular resolution in real space. As STM relies on a finite conductivity of the sample, the vast majority of studies use single crystal metal substrates. This, however, is associated with severe limitations: Electronic interactions with the metallic support can significantly affect the electronic, magnetic and conformational structure of adsorbates, thereby modifying or hampering their functionality. Furthermore, homogeneous metallic substrates usually prevent the formation of regular arrays of nanostructures. Molecules when adsorbed on a surface interact with both the substrate and coadsorbates. Depending on the resulting balance of forces, they may experience attractive or repulsive interactions between each other. At submonolayer coverage, the former case yields self-assembled islands or networks[1,2] while the latter situation leads to a homogeneous distribution of individual molecules scattered across the entire surface area.[3−5] The organized growth of arrays of assemblies, highly desirable to complement structure formation on the nanoscale, thus calls for templated surfaces exhibiting periodicities in the nanometer regime. As reconstructions on metallic

* Address correspondence to wau@tum.de.

Received for review September 5, 2013 and accepted December 2, 2013.

Published online December 11, 2013
10.1021/nn406024m

substrates only provide limited possibilities regarding periodicity and symmetry of the superstructure,[6,7] ultrathin adlayers offer new perspectives.[8] Here, special interest focuses on nonmetallic or insulating spacer layers, which reduce the electronic coupling between adsorbate and metallic substrate but are suitable for a characterization with STM, thus yielding information on nearly unperturbed properties of functional adsorbates. The application of various ultrathin oxide,[9] nitride[10] and halide[11,12] films grown on metal substrates as supports for atoms or molecules has been reported, but their considerable polarity, corrugation and structural inhomogeneity might be a drawback regarding large-scale self-assembly. As an alternative, epitaxial graphene[13−24] or boron nitride (BN)[15,21,25−29] layers recently emerged as promising nanoscale templates. Nevertheless, on insulating spacer layers, including boron nitride sheets, self-assembly protocols for the construction of advanced molecular architectures remain to date largely unexplored.

Atomically thin BN films can be grown by chemical vapor deposition from borazine on various transition metals with exquisite control of the interface structure.[30−36] As for isostructural graphene, the sp^2 sheet can exhibit a considerable geometric corrugation, resulting in nanomesh structures[32] or moiré patterns, or be planar in case of a commensurate, epitaxial fit with the substrate lattice.[30] BN's diverse topographical features on transition metals, together with its exceptional physical and chemical properties (large band gap, inertness, temperature stability), make it lucrative as substrate or template to support molecules[25,37] (vide supra) or graphene.[38−40] Recently, we have shown that BN on Cu(111) exhibits a rather unique, topographically planar, but electronically corrugated structure.[41] Apart from being an interesting spacer layer to electronically decouple functional molecules from metal supports, BN/Cu(111) features a periodically modulated surface potential, which is observed as contrast- invertible electronic moiré pattern in STM images. These moiré-like superstructures coexist with variable periodicities, depending on the rotation of the BN domains relative to the Cu(111) lattice. This provides a fascinating potential landscape to study and control the adsorption and electronic properties of complex molecules.

As exemplary functional adsorbate, we use free-base porphine (2H−P, see model in Figure 3b), a highly relevant prototype macrocycle representing the parent compound of all porphyrins. Porphyrins are extremely versatile macrocyclic species with an intriguing variety of functional properties. They are ubiquitous in biological systems: incorporated as prosthetic groups in proteins, they carry respiratory gases, provide multiple sensing functions in metabolic processes, catalyze chemical transformations, and operate in photosynthetic reaction pathways.[42] Porphyrins are similarly important in synthetic materials and supramolecular chemistry. They have been tailored for sensing purposes, medical applications, catalysis, dye-sensitized solar cells and reticular design of metal−organic frameworks.[43] From a surface science perspective, the versatile chemical termination of functionalized porphyrins allows for the self-assembly of well-defined architectures on metal supports. For example, two-dimensional (2D) porphyrin arrays and porous networks, 1D-coordination polymers and 0D supramolecules were reported.[44−52] To date, the free-base porphine has received little attention. This is surprising, as systematic studies on 2H−P could provide a reference for the entire class of porphyrins. Multimethod studies of 2H−P on Cu(110)[49] and Cu(111)[4] show an electron exchange between the substrate and the porphine. Our recent study of 2H−P on Ag(111) revealed a rather complex behavior considering the rather inert, noble metal character of the substrate. Charge transfer, preferred adsorption sites and dominating repulsive intermolecular interactions prevent island formation at submonolayer coverages and induce phase transformations.[5] In striking contrast, functionalized free-base species such as 2H-TPP arrange in well-defined assemblies even at very low coverage.[53] In brief, as the porphine is drastically modified at the molecule/metal interface, no experimental reports on intrinsic characteristics and self-assembly properties of 2H−P on surfaces are available to date. To complement the porphine data, we also applied tetracyanoquinodimethane (TCNQ), a prototype acceptor molecule, as adsorbate on the BN template.

In this article, we present a detailed study of 2H−P on BN/Cu(111). Specifically, we report three characteristics of the porphine/BN/Cu interface, which are clearly different from adsorption on metal substrates, thus highlighting the impact of the ultrathin BN spacer layer. (i) The reduced electronic coupling to the metal support results in a distinct gap of about 3.85 eV and allows us to directly visualize the frontier orbitals of 2H−P in STM images. A comparison to Density Functional Theory (DFT) and Extended Hückel Theory (EHT) calculations of the charge density of HOMO and LUMO of an isolated 2H−P reveals a good agreement, confirming the assignment of the molecular resonances and the electronic decoupling. (ii) Porphines self-assemble into well-defined agglomerates with a nearest neighbor distance of 11.3 Å. At intermediate coverage, highly regular arrays of 2H−P islands are formed, demonstrating the role of the BN/Cu(111) surface as a template for the confined growth of nanostructures. This trapping and templating mechanism yielding ordered assemblies of unprecedented extension is related to the spatial modulation in the surface potential of BN/Cu(111) and is equally operational for TCNQ. (iii) The energy alignment of the molecular electronic resonances is tuned by the lateral positioning of the 2H−P on BN/Cu(111), which also affects the electronic

gap. For high coverage, where extended chiral porous Kagomé network structures evolve, an electronic superstructure is thus imprinted in the 2H−P film.

RESULTS AND DISCUSSION

The BN/Cu(111) interface, here serving as a substrate for the adsorption of porphine and TCNQ molecules, was comprehensively characterized in previous publications relying on different experimental approaches and theoretical modeling.[41,54−56] Importantly, the BN layer shows only a minute geometric corrugation, and therefore is considered to be topographically flat. Nevertheless, a misalignment between extended BN domains and the supporting Cu lattice induces electronic superstructures that appear as moiré-like patterns in STM images recorded at high bias voltages. Specifically, circular protrusions, labeled "hills" (H) or moirons were identified as low local work function areas, which are separated by "valley" (V) and "bridge" (B) regions characterized by a higher local work function (see Figure 1a).[41,54] Here, we introduce additional experimental insight into the electronic structure of the BN/Cu(111) interface. Figure 1b represents a series of 81 d*I*/d*V* spectra recorded along a line across the surface, plotted in an energy *vs* distance map, where the d*I*/d*V* intensity is color-coded. The spectral features, appearing as bright bands in the map, reflect field emission resonances (FERs, see Figure 1c). As the energy of the FERs is related to the local work function and the surface potential,[57−60] we conclude that the BN/Cu(111) interface is characterized by a *smooth, continuous* lateral variation of the surface potential and the local work function. Figure 1b reveals considerable energy shifts of the FER's by ≈300 meV. In agreement with our previous report, the low local work function regions correspond to the H areas.[41] However, it should be noted that the energy shift of single FERs does not directly reflect the local work function difference. Only an evaluation of several resonances yields an estimate for this quantity.[58] Consistent with our previously published experimental values, the local work function on the H regions is ≈300 meV lower than that on the B or V regions. We assign all spectral features in Figure 1 to FER's and exclude important contributions of localized interface states as all peaks show consistent energy shifts when changing the tip−sample distance (see Supporting Information Figure S1).

To characterize individual porphine molecules on BN/Cu(111) and to study the initial phase of self-assembly, 2H−P was prepared with low coverage at room temperature. Figure 2c shows the site specific trapping and formation of small porphine aggregates on the H regions or moirons of the electronic BN/Cu(111) superstructure at low coverage. In contrast to porphine adsorption on Ag(111) (Figure 2a) and

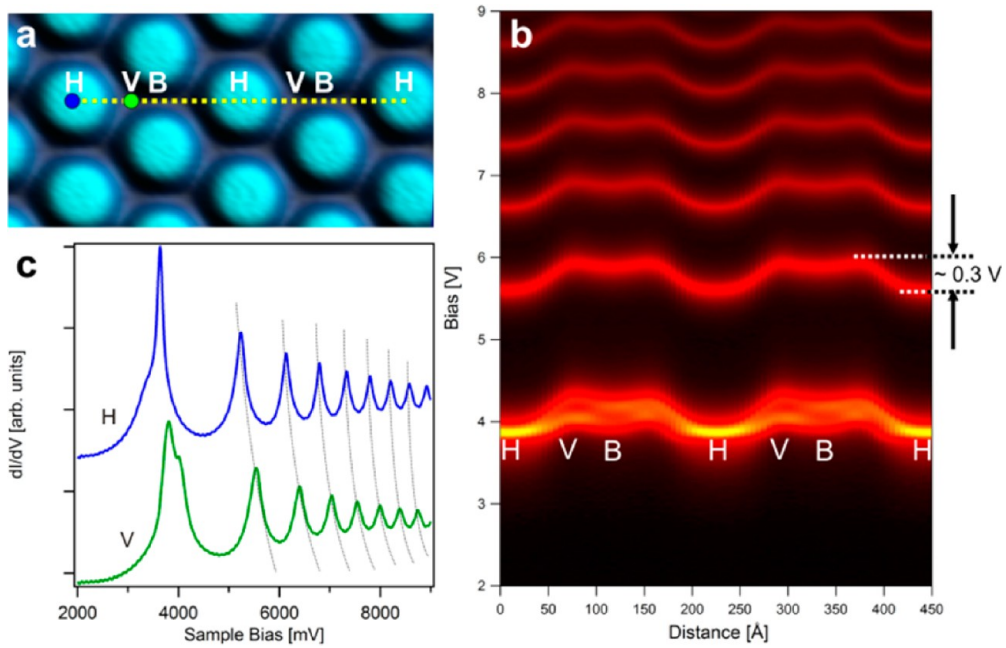

Figure 1. Electronic superstructure of the BN/Cu(111) interface. (a) STM image recorded at a bias of 4.0 V revealing circular protrusions (labeled "hills" H or moirons) separated by dimmer regions ("valley" V and "bridge" B, respectively) (*I* = 50pA).The dotted line represents the positions of 81 d*I*/d*V* spectra taken across this moiré-like superstructure. The colored dots mark two characteristic positions (H (blue) and V (green)) to describe the local surface potential at BN/Cu(111). Corresponding d*I*/d*V* spectra are shown in (c). (b) Energy *vs* distance map of the d*I*/d*V* spectra revealing a continuous spatial modulation of surface potential along the line plotted in (a). The bright bands represent field emission resonances (FERs), evidencing an energy variation of about 300 meV between H and V areas. (c) d*I*/d*V* spectra showing series of FERs on the two positions (H and V) confirm a considerable shift in energy of all resonances, consistent with a lower local work function in the H regions. The dashed lines serve as guides to the eye to highlight the shift.

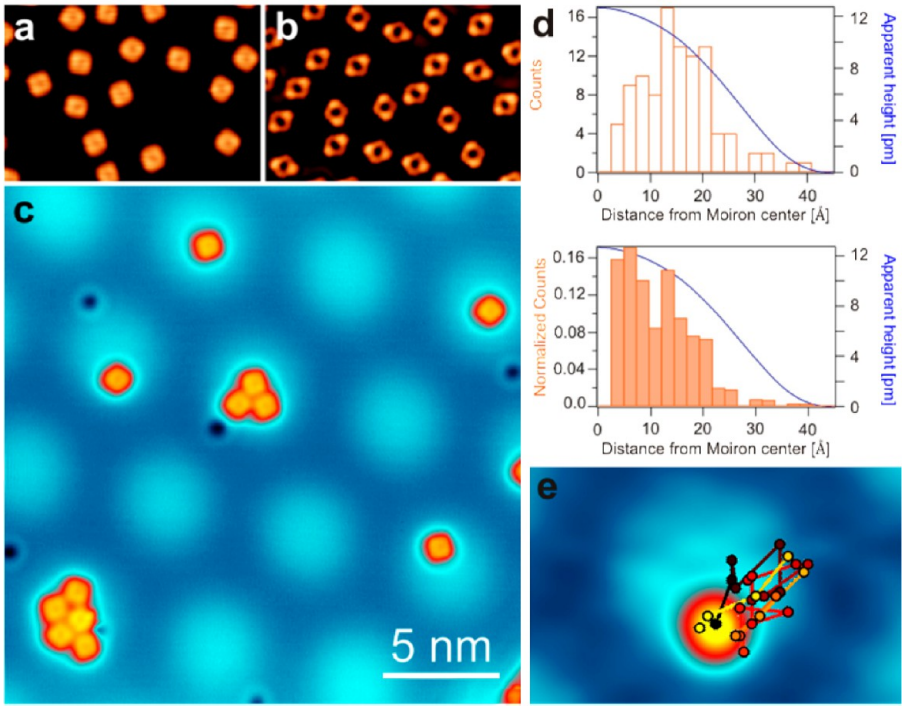

Figure 2. Trapping of 2H−P on the electronic BN/Cu(111) superstructure. On the metallic Ag(111) (a, V_b = −0.8 V, I = 200 pA) and Cu(111) (b, V_b= −0.1 V, I = 200 pA) surfaces serving as reference systems, repulsive interactions prevent the assembly of porphine aggregates at low coverage. (c) STM image showing the trapping of individual 2H−P molecules (orange squares) and small porphine aggregates on the H areas (or moirons, light blue) of the BN/Cu substrate. The formation of 2H−P islands on the BN is attributed to a reduced electronic coupling of the molecules to the Cu (V_b= 1 V, I = 30 pA). (d) A statistical analysis of the radial positions of 2H−P on the moirons reveals a preference for off-center adsorption in the raw data (top panel). Normalizing the counts with the available area, however, yields a decreasing probability of residence with increasing distance from the moiron center (bottom panel). The blue curve represents an apparent height profile from the center of a moiron to the B region. (e) Jumps of a 2H−P upon injection of electrons. The color-coded dots mark the positions of the molecule, which is trapped on the moiron.

Cu(111) (Figure 2b), where repulsive intermolecular forces prevent the assembly of aggregates below 0.88 ML,[4,5] small islands are observed on BN. The nearest neighbor distance in these aggregates amounts to 11.3 ± 0.5 Å. This value is very close to the preferred lateral in-plane separation of two 2H−P molecules calculated by simple molecular mechanics simulations (MM+) that do not include interactions with the substrate. Thus intermolecular repulsion does not play a decisive role for 2H−P/BN/Cu(111), in contrast to 2H−P in direct contact with a Cu(111) or Ag(111) substrate, where charge transfer has been reported.[4,5] This is a first indication of an effective electronic decoupling of the porphine from the metallic substrate by the BN spacer layer. Nevertheless, a considerable amount of isolated molecules is observed, seemingly trapped on the moirons or H areas of the BN/Cu(111) superstructure. Clearly, the 2H−P molecules avoid the V and B regions. A statistical analysis of the 2H−P locations on the moirons reveals a preference for off-center positions (Figure 2d, top panel). However, after normalizing the counts with the area available for adsorption, which rises linearly with increasing distance r from the moiron center, a monotonous distribution is observed (Figure 2d, bottom panel). Thus, the porphine experiences a trapping on the moirons without favored ring-like adsorption sites. This observation is corroborated by molecular manipulation experiments. Electron injection from the stationary STM tip into the lowest unoccupied molecular orbital (LUMO) induces a lateral translation of the 2H−P on the BN moiron. Tracking a molecule through a sequence of jumps visualizes the confinement on the moiron (see Figure 2e). Color-coded dots and lines, ranging from black to yellow, represent the trajectory of the molecule.

The selective confinement of molecules, clusters or atoms on specific areas of nanostructured surfaces can be triggered by the absolute value of the local work function,[6,7] the strength of van der Waals (vdW) interactions with the support,[61] the magnitude of vertical dipole moments on polar substrates,[17,62] or lateral electric fields on surfaces exhibiting a corrugated electronic potential.[19,63] In the present case, the experimentally observed distribution of individual 2H−P molecules on the moiron is consistent with an important role of the absolute value of the local work function (compare Figures 1b and 2d). However, our DFT calculations including vdW corrections show essentially no difference in the binding energy of 2H−P

on the local low- and high-work function areas corresponding to the $B_{fcc}N_{top}$ (E_{ads}= 1.93 eV) and $B_{hcp}N_{fcc}$ (E_{ads} = 1.94 eV) registries, respectively. The interaction energy of 2H−P on the large moiré cell are also rather uniform, ranging between 2.01 and 2.04 eV (see table in Figure 7d). It should be noted that the latter quantity is larger because possible relaxation of the substrate and adsorbate are not taken into consideration.[64] Irrespective of the precise mechanism, the trapping or confinement, going hand in hand with a spatial ordering of the molecules, is tentatively rationalized with the periodic modulation of the surface potential of the BN/(Cu(111) interface.

Figure 3 shows d*I*/d*V* spectra along with STM images of a single molecule. A direct comparison of spectra of 2H−P on BN (blue) with reference data of bare BN (red), 2H−P on Ag(111) (green) and Cu(111) (black) is shown in Figure 3a. The 2H−P/BN spectrum evidences pronounced resonances at −2.4 and +1.45 V, in striking contrast to the featureless spectrum of 2H−P in direct contact with a Ag(111) or Cu(111) surface. The unoccupied spectral feature cannot be described by a single peak but exhibits some fine structure. [The apparent fine structure of the LUMO resonance is influenced by the termination of the STM tip, as seen when comparing Figures 3a, 6a and S4. The latter indicates a series of side peaks, reminiscent of vibrational excitations detected for molecules adsorbed on insulating layers (see Supporting Information, Figure S4).] Consequently, we use the slope to define the apparent gap between the resonances, which amounts to about 3.5 V (dotted line in Figure 3a). Clearly, the electronic contributions in the 2H−P gap are dominated by the BN/Cu(111) substrate, which accounts for an electronic interface state (red spectrum).[41] The effective decoupling of the 2H−P from the electron-rich metal by the BN is supported by a negative differential resistance (NDR) regime trailing the unoccupied 2H−P resonance.[65] As expected from these scanning tunneling spectroscopy data, STM images of 2H−P/BN/Cu(111) show a pronounced bias dependent intramolecular contrast (Figure 3b). In the gap, the molecule appears as featureless square representing the geometric outline of 2H−P. At the energies of the resonances, the appearance of the molecule is considerably modified. The STM image representing the occupied state is dominated by four bright protrusions; for the unoccupied resonance, a two-fold symmetry prevails. This contrast is in excellent agreement with calculated charge density plots of the highest occupied (HOMO) and lowest unoccupied (LUMO) molecular orbital of an isolated 2H−P molecule. Figure 3b compares the STM images (top panel) with the HOMO and LUMO obtained from DFT calculations of an isolated 2H−P molecule (middle panel) and the corresponding constant charge density contours based on EHT simulations (bottom panel).[66] Based on the close

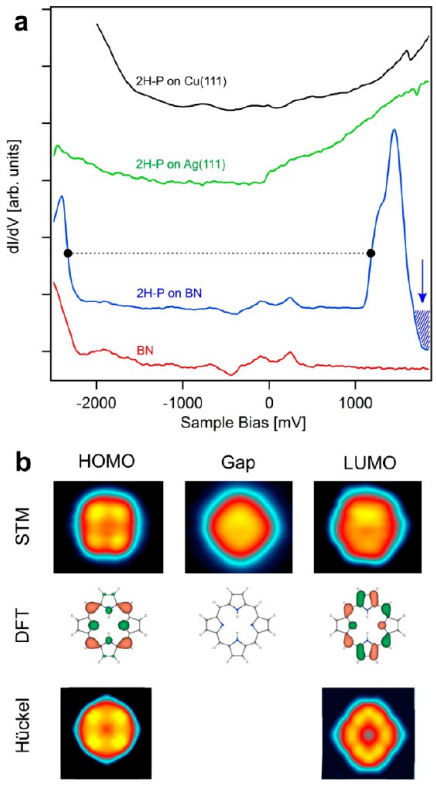

Figure 3. Electronic characterization of 2H−P on BN/Cu(111). (a) Comparative d*I*/d*V* spectra recorded on BN/Cu(111) (red), on the center of 2H−P on Ag(111) (green), Cu(111) (black) and BN/Cu(111) (blue), respectively. While contributions from the surface and interface states are observed near the Fermi energy (sample bias = 0) in all spectra, only the spectrum representing 2H−P/BN/Cu(111) shows pronounced resonances at −2.4 and 1.45 V separated by a gap. The dashed line marks the apparent electronic gap of ≈3.5 V. The NDR region highlighted in blue (see arrow) confirms a reduced electronic coupling of 2H−P to Cu. (b) The top panel represents the bias dependent appearance of 2H−P/BN in experimental constant current STM images, recorded in the gap or at the positions of the (un)occupied resonances (HOMO, V_b= −2.45 V, I = 100 pA; gap, V_b= 1 V, I = 30 pA; LUMO, V_b= 1.25 V, I = 30 pA). The STM images are well reproduced by constant charge density contours based on extended Hückel simulations (bottom panel), reflecting the HOMO and LUMO orbitals as calculated by density functional theory (DFT, middle panel). A Gaussian blurring was applied to the Hückel contours to mimic the finite resolution in the STM experiment. See text for discussion.

resemblance, the resonances identified in the 2H−P spectrum on BN can be assigned to the HOMO and LUMO orbital, respectively. Our DFT calculations yield a value of 1.93 eV for the electronic gap of isolated porphine, a quantity typically underestimated by GGA methods. Indeed, recent theoretical studies focusing on a precise determination of electronic and optical gaps in organic materials report a HOMO−LUMO gap in isolated porphine of 5.0 or 5.2 eV and emphasize the strong excitonic effects in optical spectra.[67,68] Our experimentally determined electronic gap (3.85 eV peak to peak, 3.5 eV apparent gap) is still considerably smaller than these values, evidencing some interaction of the porphine with its support.

Indeed, the binding energy of the HOMO relative to the vacuum level (~6.4 eV) is smaller than the ionization potential of 6.9 eV determined for gas phase 2H−P.[69] [The binding energy of the HOMO relative to the vacuum level is estimated by adding the binding energy of the HOMO relative to the Fermi level (2.4 eV) to the average workfunction of BN/Cu(111) (~4 eV).]

Free-base porphyrin systems contain two hydrogens in the interior of the tetrapyrrole macrocycle, which can undergo a tautomerization process.[70] Our STM data of 2H−P/BN/Cu(111) indeed show the tautomerization switching, reflected in a 90° rotation of the LUMO symmetry,[10] thus corroborating the resolution of the LUMO (*cf.* Figure S2 in the Supporting Information).

With increasing molecular coverage, the average size of the 2H−P aggregates confined to the moirons increases. Figure 4a shows a highly ordered array of 2H−P islands at a coverage of about 0.4 monolayers (ML) on a BN/Cu(111) domain characterized by a superstructure periodicity of 7 nm. [The monolayer is defined as the entire surface coverage by the Kagomé network (see Figure 5g).] The templating effect of the BN/Cu(111) substrate is clearly discernible and is also reflected in the fast Fourier transform (FFT) of the image (Figure 4b). The sharp hexagonal pattern at the center represents the inter-island distances. Remarkably, each moiron hosts an extended, self-assembled 2H−P island. An inspection of the islands'

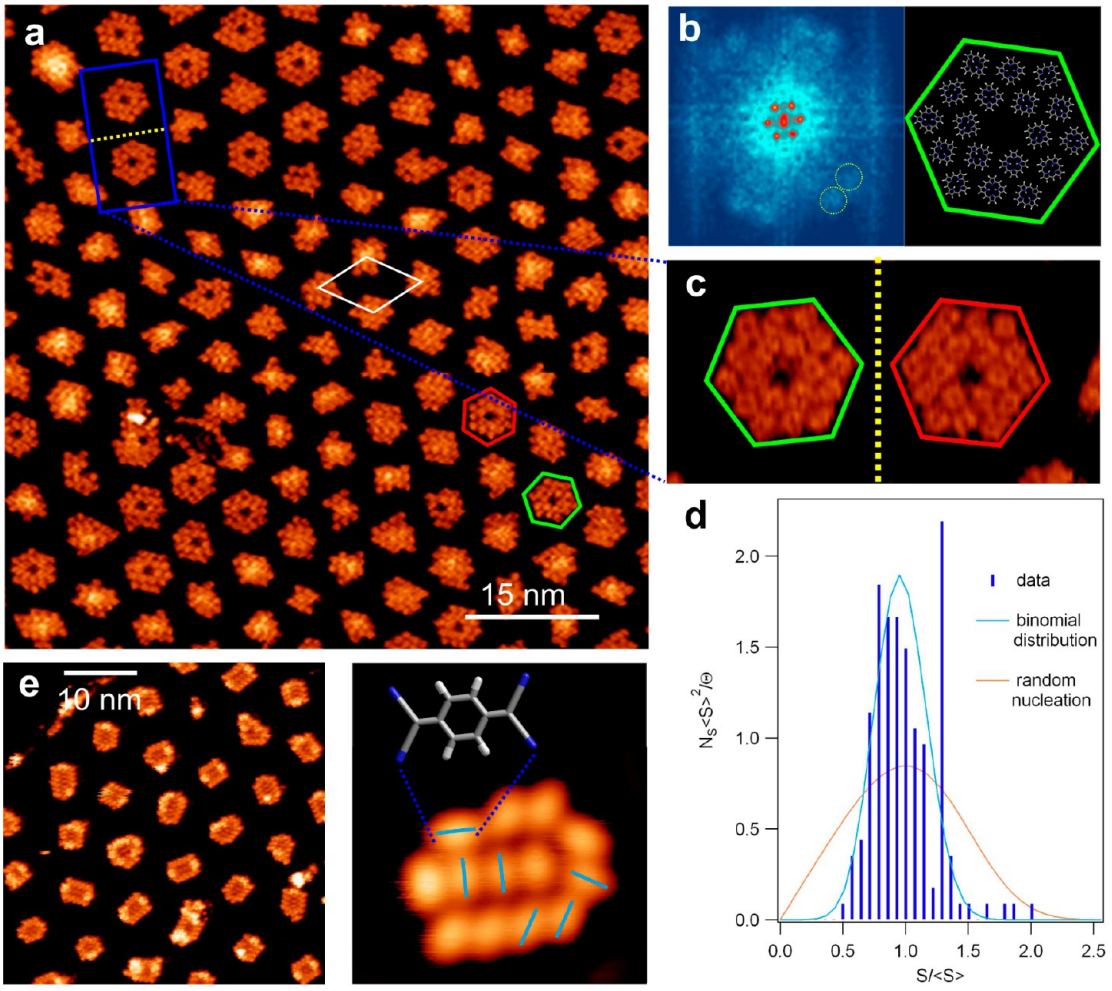

Figure 4. Templating functionality of BN/Cu(111) and island morphology. (a) STM image revealing the formation of extended self-assembled 2H−P islands at intermediate coverage confined on the moirons (V_b= 1.0 V, I = 48 pA). The most abundant assemblies, hexagonal 18-molecule islands featuring a central cavity, are marked by the green and red hexagons. (b) FFT image to highlight the structural order in (a). The six inner spots (red) reflect the order of the array, *i.e.*, the arrangement of the assemblies. The 12 outer spots (highlighted by yellow circles) represent the order within the assemblies, *i.e.*, the arrangement of the molecules and the chirality (see text for details). A model of one of the chiral hexagons (green) is shown in the right panel. (c) A zoomed and rotated segment from (a, blue rectangle) exhibits the mirror symmetric pair of chiral hexagonal assemblies (red and green). (d) Normalized island-size distribution plot for a coverage corresponding to a), clearly showing the dominance of the 18-molecule assemblies (corresponding to S/⟨S⟩ = 1.3, see text for discussion). The experimental distribution is clearly narrower than the red random nucleation curve, confirming the templating functionality of the electronic superstructure of the BN/Cu(111) interface. The cyan curve shows a binomial distribution representing perfect confinement. (e) Formation of arrays of TCNQ aggregates on BN/Cu(111) after room temperature deposition (V_b= 1.6 V, I = 21 pA). The right panel shows the molecular arrangement within one specific island and a structural model of TCNQ (V_b= 0.3 V, I = 33 pA). The solid lines (cyan) highlight the different coexisting TCNQ orientations and the relative molecular positions.

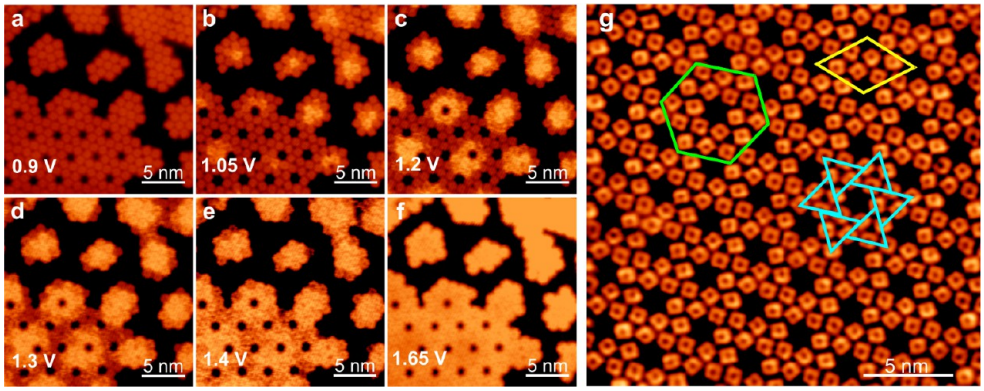

Figure 5. Bias and position dependent appearance of 2H−P on BN/Cu(111). (a−f) STM image sequence recorded with increasing bias voltage. The area represented shows the coexistence of an extended network with the ordered island phase (I = 30 pA, identical color scale). The modified appearance with increasing bias is assigned to electron transport *via* the LUMO. The lateral contrast variation is induced by the corrugated surface potential of the BN/Cu(111) interface (see text for discussion). (g) Extended porous 2H−P Kagomé network on BN/Cu(111) at high coverage (V_b= 1.0 V, I = 50 pA). Here, the templating effect is overridden. The assembly includes the hexagonal 18-molecule motif (green hexagon, compare Figure 3) and is characterized by a rhombic unit cell (highlighted in yellow).

shapes and sizes reveals repeating morphologies including a prominent hexagonal assembly formed by 18 molecules exposing a central vacancy (examples are marked by colored hexagons in Figure 4a). Indeed, the island-size distribution plot based on the analysis of 160 moirons (>2200 molecules), normalized according to scaling theory, shows a clear preference for 18-molecule clusters (see Figure 4d). Here, N_S describes the island density, θ the coverage, $S(\langle S\rangle)$ is the (average) number of molecules per island.[6,71] The strong contribution for a normalized island size $S/\langle S\rangle$ = 1.3 represents the 18-molecule clusters, corresponding nearly exclusively to the porous hexagonal assemblies. The red solid line shows the calculated size distribution from scaling theory for random nucleation (i = 1) on an isotropic substrate.[6,71] Clearly, the experimental distribution is narrower, *i.e.*, has a higher size uniformity, thus confirming the templating effect of the electronic BN/Cu(111) superstructure. Assuming a perfect confinement of deposited 2H−P molecules on the moiron cells, a binomial distribution of the island sizes is expected.[6] The cyan curve in Figure 2b bases on the binomial distribution $P_k = \binom{n}{k} p^k q^{n-k}$ relying on the experimental parameters ($p = \theta = 0.4$ is the coverage, $q = 1 - \theta$, k is the island size and n = 33 is the number of sites in a supercell (white rhombus in Figure 4a)). The agreement with the experimental size distribution is reasonable, notably concerning the width. The calculated standard deviation $\sigma = (q/np)^{1/2}$ of 0.21 compares well with values reported for templated, self-organized growth.[6] However, the binomial distribution naturally fails completely in describing the preference for the 18-molecule cluster. To rationalize the abundance of these porous hexagon-shaped assemblies, all the observed island sizes and shapes where analyzed regarding two features: First, the average number of nearest neighbors per molecule in an island and second the number of *peripheral* molecules interacting with only two neighbors, thus representing an "open shell" structure. In comparison to the porous assemblies formed by 15, 16, and 19 molecules, the porous hexagon includes no peripheral molecules and features the highest average number of nearest neighbors, making it the favored configuration. As discernible in Figure 4, the 18-molecule clusters are chiral; *i.e.*, two mirror symmetric assemblies are observed on the surface (examples are marked by the green and red hexagon, respectively). Figure 4b (right side) shows a structural model of one of the two chiral assemblies (green hexagon). Indeed, their existence is also revealed in the FFT. Twelve diffuse spots are detected at larger k values reflecting the intermolecular distance (highlighted by circles in Figure 4b, FFT image). From the hexagonal packing within one island, only six spots are expected. The 12 spots emerge from the coexistence of the two chiralities, which are due to the two equivalent possibilities to arrange two aligned 2H−P molecules relative to each other. Figure 4c shows a zoom in on a mirror symmetric chiral pair of hexagonal assemblies, marked by red and green borders.

It should be pointed out that the above analysis represents one specific BN/Cu(111) domain. Nevertheless, the conclusions about the templating function are generally valid for all superstructure periodicities and moiron sizes observed (see for example Figure 2 and Figure 5). Interestingly, the central vacancy, having a footprint of one 2H−P molecule, is not a common feature of all moirons: Some assemblies are dense-packed and larger moirons can host aggregates with several individual off-center vacancies (see Supporting Information, Figure S3a). Although we cannot clarify in detail the driving force for the vacancy formation, the porous hexagonal units are the building blocks for extended 2H−P islands prevailing at higher coverage (*vide infra*).

The potential of BN/Cu(111) as a template is also evident for a structurally and electronically distinctly

different adsorbate, namely TCNQ. Figure 4e evidences the formation of arrays of TCNQ assemblies after room temperature deposition, analogous to the 2H−P situation. STM images of individual islands (*e.g.*, Figure 4e, right panel) reveal the packing scheme of these aggregates, reminiscent of nitronaphthalene supermolecules reported on a reconstructed Au surface.[72] Judging from the molecular dimensions, the average planes of the TCNQ units adsorb parallel to the surface. Distinct molecular orientations differing by 30°, 60° or 90° coexist, representing specific intermolecular coupling motifs exhibiting a nearest neighbor separation of ≈8 Å, with a minimal N···H distance of 3 Å. A simultaneous expression of orthogonal (90°) and side-by-side (0°) arrangements was observed for TCNQ/Cu(111),[73] while parallel (0°), but offset TCNQ alignments are reported on other coinage metal surfaces.[74−76] These homogeneous metal substrates however never supported the organized growth of TCNQ arrays, but yield extended islands at submonolayer coverage. A templated TCNQ growth was achieved on graphene/Ru(0001), where the close match between moiron extension and molecular size results in individual TCNQ units at low coverage.[23]

At coverages exceeding ≈0.4 ML, the 2H−P start to form extended highly regular porous networks with a rhombic unit cell (side length of 3.2 nm) including six molecules (Figure 5g, yellow rhombus). The hexagonal 18-molecule cluster abundant at intermediate coverage is observed as repetitive motif in the porous network (green hexagon) thus demonstrating some hierarchy in the assembly. A close inspection of the extended assemblies reveals their chiral Kagomé-type structure (highlighted in cyan in Figure 5g).[77] A similar structure was reported for phthalocyanines on a graphene-based moiré pattern.[20] Obviously, the templating effect of the BN superstructure can be overridden provided the number of molecules is large enough. This is neatly apparent in Figures 5a and S3b (Supporting Information) showing phase boundaries between the confined assemblies and the extended network.

In Figure 5a−f, an image sequence recorded with increasing positive sample bias voltage (representing unoccupied electronic states) is shown. Clearly, the appearance of the 2H−P depends both on the applied voltage and the lateral position. At 0.9 V, all molecules appear with an identical contrast. At 1.05 V, the 2H−P near the center of the moirons exhibit an increased apparent height. Here, the position of the moirons or H areas in the extended network is deduced from the positions of the individual islands. While increasing the bias between 0.9 and 1.65 V, this brighter appearance of the molecules gradually spreads outward, *i.e.*, radially away from the moiron centers (Figure 5a−f). At 1.65 V, all 2H−P appear with an identical contrast again, which however is different from the situation at 0.9 V. To clarify this position- and bias-dependent contrast, d*I*/d*V* spectra were recorded above the center of porphines located at characteristic spots of the BN/Cu(111) superstructure. Figure 6a compares spectra on the center of the "hill" (blue), "in-between" (green) and the "bridge" (red), which show significant shifts of the HOMO and LUMO resonances. Importantly, the LUMO related peak of the molecules on the "hills" is shifted by about 300 mV to lower energy as compared to the "bridge", while the spectral shape is conserved. This explains the spatial-energy variation in appearance of the 2H−P molecules: First, the increased apparent height is assigned to tunneling into the LUMO of the 2H−P. Second, the radial increase in brightness with increasing bias voltage is explained by the upshift of the LUMO resonance with increasing distance from the center of the moiron.

We attribute these LUMO shifts to the smooth spatial modulation of the local surface potential of the electronic BN/Cu(111) superstructure (compare Figure 1b), where we observed an energy variation in the field emission resonances of about 300 meV between the H and V or B areas, with the lowest local work function on the moirons. The mechanism behind the energy shifts is consistent with a vacuum level alignment of the LUMO, as sketched in the diagrams reproduced in Figure 6c representing the energy level alignment for the B (red) and H (blue) positions. The LUMO energy is given by the electron affinity (E_A) relative to the vacuum level of the sample, which is defined by the local work function. Assuming E_A to be constant, the reduced local work function on the moirons (Φ_H, blue) shifts the LUMO closer to the Fermi level; *i.e.*, electrons can tunnel into the LUMO at lower bias voltages as compared to the V situation (Φ_B, red). This vacuum level alignment of molecular orbitals is consistent with an efficient electronic decoupling of the 2H−P from the metal support. Nevertheless, the voltage drop across the BN spacer layer does not drastically affect the level alignment. A variation of the tip−sample distance by 2 Å shifts the LUMO resonance by less than 50 mV, which is much smaller than the value of 300 mV reported above. A very recent study addressing phthalocyanines on a graphene/BN support also reports varying energies of molecular orbitals and assigns this effect to an spatially dependent electronic doping of the molecules.[78] For 2H−P/BN, we do not consider relevant charge transfer to/from the molecules as the 2H−P frontier orbitals do not contribute significantly to the density of states at the Fermi level (see Figure 3).

The spatially dependent energy shift is also reflected in the HOMO resonance, which appears as a distinct step-like feature in the negative sample bias regime (Figure 6a). It shows the same trend as the LUMO. However, the HOMO−LUMO gap varies depending on the 2H−P position on the superstructure.

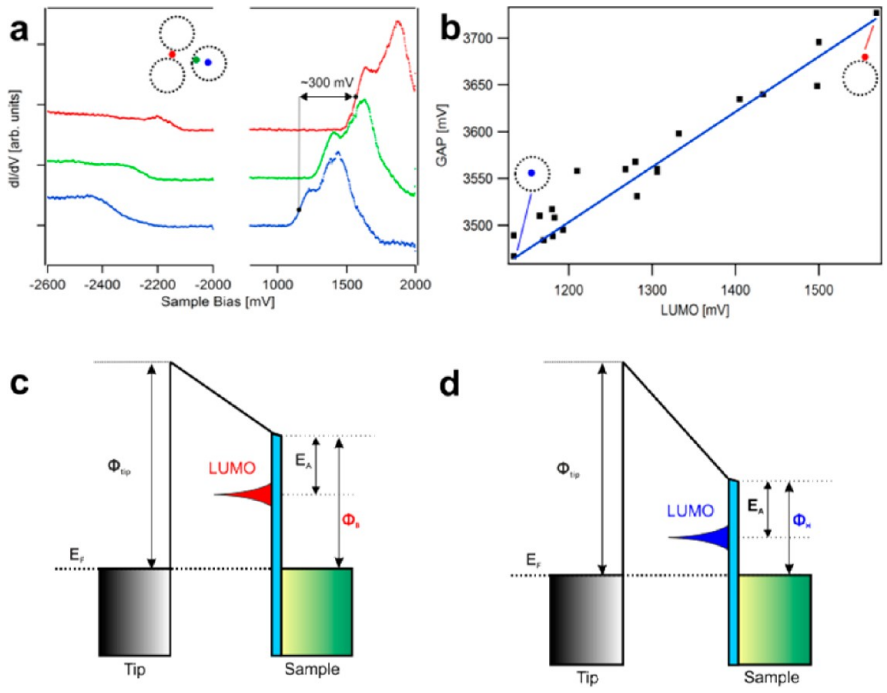

Figure 6. Position-dependent energy level alignment of 2H−P on BN/Cu(111). (a) d*I*/d*V* spectra recorded above the center of porphines positioned on characteristic sites of the superstructure: center of the moiron (blue marker and spectrum), rim of the moiron (green marker and spectrum), and B area (red marker and spectrum).The energy of the LUMO varies by about 300 mV between the H and V positions. (b) Change of the HOMO−LUMO gap of 2H−P for different positions on the superstructure (see text for discussion). (c and d) Models sketching the tip−sample interface for the high (c: H) and the low local work function areas (d: V, B). A vacuum level alignment of the LUMO combined with a constant electron affinity E_A brings the LUMO energy on the moiron closer to the Fermi level and thus explains the observed shifts in the d*I*/d*V* spectra as well as the spatially inhomogeneous contrast in STM images recorded between 1 and 1.4 V (compare Figure 5) (see text for further discussion).

The molecules have the smallest gap on the "hills" and the largest on the "valleys". Figure 6b evidence a linear dependence of the HOMO−LUMO gap on the LUMO position and the lateral position, respectively. Thus, a rigid band shift due to a vacuum level alignment does not precisely describe the real situation, despite being a reasonable approximation. We tentatively assign the variation of the gap to subtle modulations of the molecule−substrate interactions, *i.e.*, to screening effects.[79,80] Compared to the high local work function areas, the low local work function regions (H) facilitate an electronic interaction with the underlying metal and thus enhance the screening, which is reflected in a reduced HOMO−LUMO gap. Indeed, the confinement of 2H−P on the moirons at low and intermediate coverage, evidencing an increased interaction with the support, is consistent with this interpretation.

The electronic structure of 2H−P on various positions across the moiré cell as obtained from DFT calculations shows a similar behavior. We have previously demonstrated that the spatial variation of the local work function can be rationalized with the modulation of the adsorption registry of BN on Cu(111).[54] Here we placed the molecule on 6 positions along the diagonal of the moiré cell where the electronic corrugation is strongest (Figure 7a). We plot the p_z density of states, projected on the C and N atoms at each of these positions (Figure 7b) to elucidate the local variation of the electronic structure. The positions of the HOMO and LUMO are modulated depending on the placement of the adsorbate. In particular, at point I ("hill" H) the orbitals are shifted to the lowest and at point IV ("valley" V) to the highest energies. The overall spread of the orbital energies amounts to 100 meV, noticeably smaller than what is observed in the STS. Looking at the LUMO positions (projected onto C atoms) more closely (Figure 7c), it becomes evident that the orbital energies are strongly linked to the surface electrostatic potential (ESP), and thus to the local work function at the height of the porphine molecule. The LUMO position closely follows the variation in the ESP, where 2H−P in positions with a low ESP shows a LUMO peak at lower energies, while high ESP causes an upshift of the LUMO. Qualitatively, the DFT results reproduce the LUMO shifts measured with STS (*cf.* Figure 6a), while the overall variation is smaller by a factor ~3. This is consistent with the underestimated magnitude of the electronic corrugation. Also spatially the calculations agree well with the points sampled by STS, finding the lowest LUMO for the H area and an increase as one moves away from the hill.

CONCLUSION

In conclusion, we presented a comprehensive STM/STS characterization of an archetypical porphyrin compound on an electronically nanostructured BN/Cu(111)

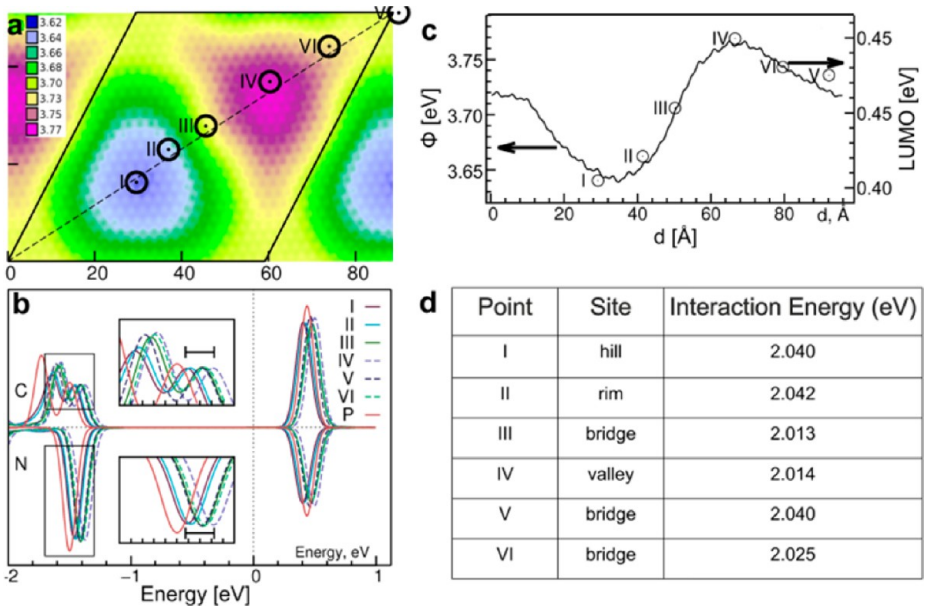

Point	Site	Interaction Energy (eV)
I	hill	2.040
II	rim	2.042
III	bridge	2.013
IV	valley	2.014
V	bridge	2.040
VI	bridge	2.025

Figure 7. DFT investigation of porphine at several adsorption sites on the BN/Cu(111) moiré. (a) Location of six adsorption positions where the 2H−P molecule was placed, superimposed on a map of the local work function (in eV) at the approximate height of the 2H−P molecule (3.3 Å above BN surface). (b) Projected density of states (p_z) of porphine-C (top) and porphine-N (bottom) atoms with 2H−P placed at various positions as indicated in (a). The PDOS of 2H−P in vacuum is plotted for comparison (curve "P"). Insets show zooms of the framed HOMO regions, scale bar indicates 100 meV. (c) Local work function (eV, line) across the diagonal of the moiré cell and positions of the LUMO maximum (eV, points) for six positions along this diagonal. (d) Interaction energy between molecule and substrate at the various locations of the BN/Cu(111) superstructure.

support. As corroborated by complementary DFT modeling, the ultrathin BN spacer layer introduces manifold new prospects as compared to conventional adsorption on metal supports. A reduced electronic coupling of 2H−P to metallic states is evidenced by the opening of an electronic gap, the resolution of frontier orbitals in STS and STM, enabling the visualization of the tautomerization-induced LUMO-switching, and the electronic level alignment. Coverage dependent studies show a trapping and ordering of 2H−P on the low local work function regions of BN/Cu(111). At intermediate coverage, this templating effect induces the unprecedented organized growth of ordered arrays of molecular assemblies, both for 2H−P and distinctly different TCNQ adsorbates. At elevated porphine coverage, extended porous chiral Kagomé networks are formed. Importantly, the lateral modulation of the surface potential at the BN/Cu(111) interface induces a periodic, spatial modulation of the energy of 2H−P frontier orbitals. This opens up the opportunity to steer the level alignment and to tune the electronic gap of surface anchored functional molecules. Thus, as exemplified by the 2H−P/BN/Cu(111) model system, the electronically corrugated BN/Cu(111) substrate introduces a fascinating potential landscape, making it a unique template to position adsorbates or fabricate functional nanostructures.

Note added: while revising the manuscript, we became aware of a recently published article[81] addressing properties of Co-phthalocyanine on a closely related h-BN/Ir(111) substrate, where very similar effects have been demonstrated, corroborating the general importance of the presently reported templating and electronic effects.

METHODS

The experiments were performed using a CreaTec STM (www.lt-stm.com) operating at 6 K under ultrahigh vacuum conditions. The BN spacer layer was prepared by chemical vapor deposition (CVD) of borazine $(HBNH)_3$ following a protocol described in detail in previous reports.[30,41,82] The 2H−P (Frontier Scientific, purity >95%) and TCNQ (Aldrich, purified by the Ruben group at Karlsruhe Institute of Technology) molecules were deposited using organic molecular beam epitaxy (OMBE) from a quartz container held at 470 or 390 K, respectively. During deposition, the BN/Cu/(111) substrate was usually kept at room temperature. All STM images were recorded in constant current mode and the differential conductance (d*I*/d*V*) spectra or scanning tunneling spectra (STS) were taken using a lock-in amplifier (f = 969 Hz, ΔV_{rms}= 18 mV). The feedback loop was closed for the field emission resonance measurements.[41] The FFT and the STM images were processed using the WSxM software.[83]

Complementary DFT calculations were carried out in order to increase our understanding of the system. Our approach uses the Gaussian plane wave formalism as available in the Quick-Step module in the CP2K package[84] and a computational setup that we have described in previous work.[41,54,64] Double-zeta MOLOPT basis sets[85] were used for all elements, with a plane-wave cutoff of 500 Ry for the electron density. The revPBE[86] exchange-correlation functional was used together with the DFT-D3 dispersion correction.[87] Projected Density of States (PDOS) curves are smoothed with a Gaussian convolution with

a width of 0.05 eV for better readability and comparability. Using this setup, we calculated the HOMO and LUMO of an isolated 2H−P molecule and these are presented in Figure 1b. The appearance and qualitative features of the orbitals are robust to changes of the exchange-correlation functional and variations of the geometry. The plots were generated using the VisIt suite, version 2.6.2.[88]

Two complementary approaches were used to model the adsorption system. First, porphine was placed atop commensurate BN/Cu(111), with the monolayer in different registries[64] ($N_{top}B_{fcc}$, $N_{fcc}B_{hcp}$) in order to model the different environments of the moiré layer.[54] Subsequently, full geometry optimizations of these systems were carried out. Second, to probe the properties of porphine on a large moiré cell, we used a 24 × 24 rotated BN layer on a 23 × 23 × 4 Cu(111) slab, as presented previously.[55] The porphine was placed at the "optimal" height determined from the geometry relaxation on various lateral positions on above the monolayer (Figure 7) and energy calculations were carried out. In all but two instances, the residual average force on the porphine molecule was smaller than 10^{-4} hartree/bohr. Where this was not the case, the vertical distance of the porphine was rigidly adjusted by at most 0.1 Å until the forces were below that threshold. Due to the prohibitive computational cost of full geometry optimizations of such a large system, this manual approach serves as an acceptable substitute.

Conflict of Interest: The authors declare no competing financial interest.

Supporting Information Available: Additional experimental STM and STS data. This material is available free of charge *via* the Internet at http://pubs.acs.org.

Acknowledgment. We thank Florian Klappenberger, Carlos Andre Palma and Nenad Kepcija for fruitful discussions. We acknowledge the purification of the commercial TCNQ compound by the Ruben group at KIT. This work is supported by the ERC Advanced Grant MolArt (no. 247299), the Munich Center for Advanced Photonics (MAP) and the Technische Universität München – Institute for Advanced Study, funded by the German Excellence Initiative. R.K., A.P.S., and J.H. are grateful for support from the Swiss National Science Foundation (Grant No. 140441) and the Swiss National Supercomputing Center (Grants s89, s425).

REFERENCES AND NOTES

1. Barth, J. V. Molecular Architectonic on Metal Surfaces. *Annu. Rev. Phys. Chem.* **2007**, *58*, 375–407.
2. Barth, J. V.; Costantini, G.; Kern, K. Engineering Atomic and Molecular Nanostructures at Surfaces. *Nature* **2005**, *437*, 671–679.
3. Stadler, C.; Hansen, S.; Krüger, I.; Kumpf, C.; Umbach, E. Tuning Intermolecular Interaction in Long-Range-Ordered Submonolayer Organic Films. *Nat. Phys.* **2009**, *5*, 153–158.
4. Diller, K.; Klappenberger, F.; Allegretti, F.; Papageorgiou, A. C.; Fischer, S.; Wiengarten, A.; Joshi, S.; Seufert, K.; Ecija, D.; Auwärter, W.; *et al.* Investigating the Molecule-Substrate Interaction of Prototypic Tetrapyrrole Compounds: Adsorption and Self-Metalation of Porphine on Cu(111). *J. Chem. Phys.* **2013**, *138*, 154710-1–154710-9.
5. Bischoff, F.; Seufert, K.; Auwärter, W.; Joshi, S.; Vijayaraghavan, S.; Écija, D.; Diller, K.; Papageorgiou, A. C.; Fischer, S.; Allegretti, F.; *et al.* How Surface Bonding and Repulsive Interactions Cause Phase Transformations: Ordering of a Prototype Macrocyclic Compound on Ag (111). *ACS Nano* **2013**, *7*, 3139–3149.
6. Brune, H.; Giovannini, M.; Bromann, K.; Kern, K. Self-Organized Growth of Nanostructure Arrays on Strain-Relief Patterns. *Nature* **1998**, *394*, 451–453.
7. Ruffieux, P.; Aït-Mansour, K.; Bendounan, A.; Fasel, R.; Patthey, L.; Gröning, P.; Gröning, O. Mapping the Electronic Surface Potential of Nanostructured Surfaces. *Phys. Rev. Lett.* **2009**, *102*, 086807.
8. Gruznev, D. V.; Matetskiy, A. V.; Bondarenko, L. V.; Utas, O. A.; Zotov, A. V.; Saranin, A. A.; Chou, J. P.; Wei, C. M.; Lai, M. Y.; Wang, Y. L. Stepwise Self-Assembly of C60 Mediated by Atomic Scale Moire Magnifiers. *Nat. Commun.* **2013**, *4*, 1679.
9. Qiu, X. H.; Nazin, G. V.; Ho, W. Vibrationally Resolved Fluorescence Excited with Submolecular Precision. *Science* **2003**, *299*, 542–546.
10. Hirjibehedin, C. F.; Lin, C.-Y.; Otte, A. F.; Ternes, M.; Lutz, C. P.; Jones, B. A.; Heinrich, A. J. Large Magnetic Anisotropy of a Single Atomic Spin Embedded in a Surface Molecular Network. *Science* **2007**, *317*, 1199–1203.
11. Liljeroth, P.; Repp, J.; Meyer, G. Current-Induced Hydrogen Tautomerization and Conductance Switching of Naphthalocyanine Molecules. *Science* **2007**, *317*, 1203–1206.
12. Repp, J.; Meyer, G.; Stojkovic, S. M.; Gourdon, A.; Joachim, C. Molecules on Insulating Films: Scanning-Tunneling Microscopy Imaging of Individual Molecular Orbitals. *Phys. Rev. Lett.* **2005**, *94*, 026803.
13. Barja, S.; Garnica, M.; Hinarejos, J. J.; Vazquez de Parga, A. L.; Martin, N.; Miranda, R. Self-Organization of Electron Acceptor Molecules on Graphene. *Chem. Commun.* **2010**, *46*, 8198–8200.
14. Wang, Q. H.; Hersam, M. C. Room-Temperature Molecular-Resolution Characterization of Self-Assembled Organic Monolayers on Epitaxial Graphene. *Nat. Chem.* **2009**, *1*, 206–211.
15. Pollard, A. J.; Perkins, E. W.; Smith, N. A.; Saywell, A.; Goretzki, G.; Phillips, A. G.; Argent, S. P.; Sachdev, H.; Müller, F.; Hüfner, S.; *et al.* Supramolecular Assemblies Formed on an Epitaxial Graphene Superstructure. *Angew. Chem., Int. Ed.* **2010**, *49*, 1794–1799.
16. N' Diaye, A. T.; Bleikamp, S.; Feibelman, P. J.; Michely, T. Two-Dimensional Ir Cluster Lattice on a Graphene Moiré on Ir(111). *Phys. Rev. Lett.* **2006**, *97*, 215501.
17. Lin, X.; Nilius, N. Self-Assembly of MgPc Molecules on Polar FeO Thin Films. *J. Phys. Chem. C* **2008**, *112*, 15325–15328.
18. Zhou, H. T.; Mao, J. H.; Li, G.; Wang, Y. L.; Feng, X. L.; Du, S. X.; Mullen, K.; Gao, H. J. Direct Imaging of Intrinsic Molecular Orbitals Using Two-Dimensional, Epitaxially-Grown, Nanostructured Graphene for Study of Single Molecule and Interactions. *App. Phys. Lett.* **2011**, *99*, 153101-1–153101-3.
19. Zhang, H. G.; Sun, J. T.; Low, T.; Zhang, L. Z.; Pan, Y.; Liu, Q.; Mao, J. H.; Zhou, H. T.; Guo, H. M.; Du, S. X.; *et al.* Assembly of Iron Phthalocyanine and Pentacene Molecules on a Graphene Monolayer Grown on Ru(0001). *Phys. Rev. B* **2011**, *84*, 245436.
20. Mao, J.; Zhang, H.; Jiang, Y.; Pan, Y.; Gao, M.; Xiao, W.; Gao, H. J. Tunability of Supramolecular Kagome Lattices of Magnetic Phthalocyanines Using Graphene-Based Moiré Patterns as Templates. *J. Am. Chem. Soc.* **2009**, *131*, 14136–14137.
21. Wang, B.; Bocquet, M.-L. Monolayer Graphene and H-Bn on Metal Substrates as Versatile Templates for Metallic Nanoclusters. *J. Phys. Chem. Lett.* **2011**, *2*, 2341–2345.
22. Wang, B.; Yoon, B.; König, M.; Fukamori, Y.; Esch, F.; Heiz, U.; Landman, U. Size-Selected Monodisperse Nanoclusters on Supported Graphene: Bonding, Isomerism, and Mobility. *Nano Lett.* **2012**, *12*, 5907–5912.
23. Garnica, M.; Stradi, D.; Barja, S.; Calleja, F.; Diaz, C.; Alcami, M.; Martin, N.; Vazquez de Parga, A. L.; Martin, F.; Miranda, R. Long-Range Magnetic Order in a Purely Organic 2d Layer Adsorbed on Epitaxial Graphene. *Nat. Phys.* **2013**, *9*, 368–374.
24. Hämäläinen, S. K.; Stepanova, M.; Drost, R.; Liljeroth, P.; Lahtinen, J.; Sainio, J. Self-Assembly of Cobalt-Phthalocyanine Molecules on Epitaxial Graphene on Ir(111). *J. Phys. Chem. C* **2012**, *116*, 20433–20437.
25. Berner, S.; Corso, M.; Widmer, R.; Gröning, O.; Laskowski, R.; Blaha, P.; Schwarz, K.; Goriachko, A.; Over, H.; Gsell, S.; *et al.* Boron Nitride Nanomesh: Functionality from a Corrugated Monolayer. *Angew. Chem., Int. Ed.* **2007**, *119*, 5207–5211.
26. Ng, M. L.; Preobrajenski, A. B.; Zakharov, A. A.; Vinogradov, A. S.; Krasnikov, S. A.; Cafolla, A. A.; Mårtensson, N. Effect of Substrate Nanopatterning on the Growth and Structure of Pentacene Films. *Phys. Rev. B* **2010**, *81*, 115449.

27. Kahle, S.; Deng, Z.; Malinowski, N.; Tonnoir, C.; Forment-Aliaga, A.; Thontasen, N.; Rinke, G.; Le, D.; Turkowski, V.; Rahman, T. S.; *et al.* The Quantum Magnetism of Individual Manganese-12-acetate Molecular Magnets Anchored at Surfaces. *Nano Lett.* **2011**, *12*, 518–521.
28. Koch, H. P.; Laskowski, R.; Blaha, P.; Schwarz, K. Adsorption of Small Gold Clusters on the H-Bn/Rh(111) Nanomesh. *Phys. Rev. B* **2012**, *86*, 155404.
29. Natterer, F. D.; Patthey, F. O.; Brune, H. Ring State for Single Transition Metal Atoms on Boron Nitride on Rh (111). *Phys. Rev. Lett.* **2012**, *109*, 066101.
30. Auwärter, W.; Kreutz, T. J.; Greber, T.; Osterwalder, J. Xpd and Stm Investigation of Hexagonal Boron Nitride on Ni(111). *Surf. Sci.* **1999**, *429*, 229–236.
31. Ćavar, E.; Westerström, R.; Mikkelsen, A.; Lundgren, E.; Vinogradov, A. S.; Ng, M. L.; Preobrajenski, A. B.; Zakharov, A. A.; Mårtensson, N. A Single H-Bn Layer on Pt(111). *Surf. Sci.* **2008**, *602*, 1722–1726.
32. Corso, M.; Auwärter, W.; Muntwiler, M.; Tamai, A.; Greber, T.; Osterwalder, J. Boron Nitride Nanomesh. *Science* **2004**, *303*, 217–220.
33. Goriachko, A.; He; Knapp, M.; Over, H.; Corso, M.; Brugger, T.; Berner, S.; Osterwalder, J.; Greber, T. Self-Assembly of a Hexagonal Boron Nitride Nanomesh on Ru(0001). *Langmuir* **2007**, *23*, 2928–2931.
34. Morscher, M.; Corso, M.; Greber, T.; Osterwalder, J. Formation of Single Layer H-Bn on Pd(111). *Surf. Sci.* **2006**, *600*, 3280–3284.
35. Müller, F.; Hüfner, S.; Sachdev, H.; Laskowski, R.; Blaha, P.; Schwarz, K. Epitaxial Growth of Hexagonal Boron Nitride on Ag(111). *Phys. Rev. B* **2010**, *82*, 113406.
36. Vinogradov, N. A.; Zakharov, A. A.; Ng, M. L.; Mikkelsen, A.; Lundgren, E.; Martensson, N.; Preobrajenski, A. B. One-Dimensional Corrugation of the H-Bn Monolayer on Fe-(110). *Langmuir* **2011**, *28*, 1775–1781.
37. Muntwiler, M.; Auwärter, W.; Seitsonen, A. P.; Osterwalder, J.; Greber, T. Rocking Motion Induced Charging of C60 on H-Bn/Ni(111). *Phys. Rev. B* **2005**, *71*, 241401.
38. Dean, C. R.; Young, A. F.; Meric, I.; Lee, C.; Wang, L.; Sorgenfrei, S.; Watanabe, K.; Taniguchi, T.; Kim, P.; Shepard, K. L.; *et al.* Boron Nitride Substrates for High-Quality Graphene Electronics. *Nat. Nanotechnol.* **2010**, *5*, 722–726.
39. Xue, J.; Sanchez-Yamagishi, J.; Bulmash, D.; Jacquod, P.; Deshpande, A.; Watanabe, K.; Taniguchi, T.; Jarillo-Herrero, P.; LeRoy, B. J. Scanning Tunnelling Microscopy and Spectroscopy of Ultra-Flat Graphene on Hexagonal Boron Nitride. *Nat. Mater.* **2010**, *10*, 282–285.
40. Decker, R. g.; Wang, Y.; Brar, V. W.; Regan, W.; Tsai, H.-Z.; Wu, Q.; Gannett, W.; Zettl, A.; Crommie, M. F. Local Electronic Properties of Graphene on a Bn Substrate Via Scanning Tunneling Microscopy. *Nano Lett.* **2011**, *11*, 2291–2295.
41. Joshi, S.; Ecija, D.; Koitz, R.; Iannuzzi, M.; Seitsonen, A. P.; Hutter, J.; Sachdev, H.; Vijayaraghavan, S.; Bischoff, F.; Seufert, K.; *et al.* Boron Nitride on Cu(111): An Electronically Corrugated Monolayer. *Nano Lett.* **2012**, *12*, 5821–5828.
42. Milgrom, L. R.; Warren, M. J. *The Colours of Life: An Introduction to the Chemistry of Porphyrins and Related Compounds*; Oxford University Press: Oxford, 1997.
43. Kadish, K. M.; Smith, K. M.; Guilard, R. *The Porphyrin Handbook: Inorganic, Organometallic and Coordination Chemistry*; Academic Press: San Diego, CA, 2003; Vol. 3, access online via Elsevier.
44. Auwärter, W.; Weber-Bargioni, A.; Riemann, A.; Schiffrin, A.; Gröning, O.; Fasel, R.; Barth, J. V. Self-Assembly and Conformation of Tetrapyridyl-Porphyrin Molecules on Ag(111). *J. Chem. Phys.* **2006**, *124*, 194708-1–194708-6.
45. Auwärter, W.; Weber-Bargioni, A.; Brink, S.; Riemann, A.; Schiffrin, A.; Ruben, M.; Barth, J. V. Controlled Metalation of Self-Assembled Porphyrin Nanoarrays in Two Dimensions. *ChemPhysChem* **2007**, *8*, 250–254.
46. Heim, D.; Seufert, K.; Auwärter, W.; Aurisicchio, C.; Fabbro, C.; Bonifazi, D.; Barth, J. V. Surface-Assisted Assembly of Discrete Porphyrin-Based Cyclic Supramolecules. *Nano Lett.* **2009**, *10*, 122–128.
47. Heim, D.; Écija, D.; Seufert, K.; Auwärter, W.; Aurisicchio, C.; Fabbro, C.; Bonifazi, D.; Barth, J. V. Self-Assembly of Flexible One-Dimensional Coordination Polymers on Metal Surfaces. *J. Am. Chem. Soc.* **2010**, *132*, 6783–6790.
48. Jung, T. A.; Schlittler, R. R.; Gimzewski, J. K. Conformational Identification of Individual Adsorbed Molecules with the STM. *Nature* **1997**, *386*, 696–698.
49. Dyer, M. S.; Robin, A.; Haq, S.; Raval, R.; Persson, M.; Klimeš, J. Understanding the Interaction of the Porphyrin Macrocycle to Reactive Metal Substrates: Structure, Bonding, and Adatom Capture. *ACS Nano* **2011**, *5*, 1831–1838.
50. Stark, M.; Ditze, S.; Drost, M.; Buchner, F.; Steinrück, H.-P.; Marbach, H. Coverage Dependent Disorder-Order Transition of 2h-Tetraphenylporphyrin on Cu(111). *Langmuir* **2013**, *29*, 4104–4110.
51. Haq, S.; Hanke, F.; Dyer, M. S.; Persson, M.; Iavicoli, P.; Amabilino, D. B.; Raval, R. Clean Coupling of Unfunctionalized Porphyrins at Surfaces to Give Highly Oriented Organometallic Oligomers. *J. Am. Chem. Soc.* **2011**, *133*, 12031–12039.
52. In't Veld, M.; Iavicoli, P.; Haq, S.; Amabilino, D. B.; Raval, R. Unique Intermolecular Reaction of Simple Porphyrins at a Metal Surface Gives Covalent Nanostructures. *Chem. Commun.* **2008**, 1536–1538.
53. Auwärter, W.; Seufert, K.; Bischoff, F.; Ecija, D.; Vijayaraghavan, S.; Joshi, S.; Klappenberger, F.; Samudrala, N.; Barth, J. V. A Surface-Anchored Molecular Four-Level Conductance Switch Based on Single Proton Transfer. *Nat. Nanotechnol.* **2012**, *7*, 41–46.
54. Koitz, R.; Seitsonen, A. P.; Iannuzzi, M.; Hutter, J. Structural and Electronic Properties of a Large-Scale Moire Pattern of Hexagonal Boron Nitride on Cu(111) Studied with Density Functional Theory. *Nanoscale* **2013**, *5*, 5589–5595.
55. Preobrajenski, A. B.; Vinogradov, A. S.; Mårtensson, N. Monolayer of H-Bn Chemisorbed on Cu(111) and Ni(111): The Role of the Transition Metal 3d States. *Surf. Sci.* **2005**, *582*, 21–30.
56. Roth, S.; Matsui, F.; Greber, T.; Osterwalder, J. Chemical Vapor Deposition and Characterization of Aligned and Incommensurate Graphene/Hexagonal Boron Nitride Heterostack on Cu(111). *Nano Lett.* **2013**, *13*, 2668–2675.
57. Binnig, G.; Frank, K. H.; Fuchs, H.; Garcia, N.; Reihl, B.; Rohrer, H.; Salvan, F.; Williams, A. R. Tunneling Spectroscopy and Inverse Photoemission: Image and Field States. *Phys. Rev. Lett.* **1985**, *55*, 991–994.
58. Coombs, J.; Gimzewski, J. Fine Structure in Field Emission Resonances at Surfaces. *J. Microsc.* **1988**, *152*, 841–851.
59. Ruggiero, C. D.; Choi, T.; Gupta, J. A. Tunneling Spectroscopy of Ultrathin Insulating Films: CuN on Cu(100). *App. Phys. Lett.* **2007**, 91.
60. Pivetta, M.; Patthey, F.; Stengel, M.; Baldereschi, A.; Schneider, W.-D. Local Work Function Moire Pattern on Ultrathin Ionic Films: Nacl on Ag (100). *Phys. Rev. B* **2005**, *72*, 115404.
61. Roos, M.; Künzel, D.; Uhl, B.; Huang, H.-H.; Brandao Alves, O.; Hoster, H. E.; Gross, A.; Behm, R. J. Hierarchical Interactions and Their Influence upon the Adsorption of Organic Molecules on a Graphene Film. *J. Am. Chem. Soc.* **2011**, *133*, 9208–9211.
62. Rienks, E. D. L.; Nilius, N.; Rust, H.-P.; Freund, H.-J. Surface Potential of a Polar Oxide Film: FeO on Pt(111). *Phys. Rev. B* **2005**, *71*, 241404.
63. Dil, H.; Lobo-Checa, J.; Laskowski, R.; Blaha, P.; Berner, S.; Osterwalder, J.; Greber, T. Surface Trapping of Atoms and Molecules with Dipole Rings. *Science* **2008**, *319*, 1824–1826.
64. Gómez Díaz, J.; Ding, Y.; Koitz, R.; Seitsonen, A. P.; Iannuzzi, M.; Hutter, J. Hexagonal Boron Nitride on Transition Metal Surfaces. *Theor. Chem. Acc.* **2013**, *132*, 1–17.
65. Franke, K. J.; Schulze, G.; Henningsen, N.; Fernández-Torrente, I.; Pascual, J. I.; Zarwell, S.; Rück-Braun, K.; Cobian, M.; Lorente, N. Reducing the Molecule-Substrate Coupling in C{60}-Based Nanostructures by Molecular Interactions. *Phys. Rev. Lett.* **2008**, *100*, 036807.
66. Gröning, O.; Fasel, R. *STM Generator Software*; EMPA Materials Science and Technology: Switzerland, 2004.

67. Palummo, M.; Hogan, C.; Sottile, F.; Bagalá, P.; Rubio, A. *Ab Initio* Electronic and Optical Spectra of Free-Base Porphyrins: The Role of Electronic Correlation. *J. Chem. Phys.* **2009**, *131*, 084102.
68. Dabo, I.; Ferretti, A.; Park, C.-H.; Poilvert, N.; Li, Y.; Cococcioni, M.; Marzari, N. Donor and Acceptor Levels of Organic Photovoltaic Compounds from First Principles. *Phys. Chem. Chem. Phys.* **2013**, *15*, 685–695.
69. Dupuis, P.; Roberge, R.; Sandorfy, C. The Very Low Ionization Potentials of Porphyrins and the Possible Role of Rydberg States in Photosynthesis. *Chem. Phys. Lett.* **1980**, *75*, 434–437.
70. Hennig, J.; Limbach, H.-H. Kinetic Study of Hydrogen Tunnelling in Meso-Tetraphenylporphine by Nuclear Magnetic Resonance Lineshape Analysis and Selective T1-Relaxation Time Measurements. *J. Chem. Soc., Faraday Trans.* **1979**, *75*, 752–766.
71. Amar, J. G.; Family, F. Critical Cluster Size: Island Morphology and Size Distribution in Submonolayer Epitaxial Growth. *Phys. Rev. Lett.* **1995**, *74*, 2066–2069.
72. Böhringer, M.; Morgenstern, K.; Schneider, W. D.; Wühn, M.; Wöll, C.; Berndt, R. Self-Assembly of L-Nitronaphthalene on Au(111). *Surf. Sci.* **2000**, *444*, 199–210.
73. Kamna, M. M.; Graham, T. M.; Love, J. C.; Weiss, P. S. Strong Electronic Perturbation of the Cu{111} Surface by 7,7′,8,8′-Tetracyanoquinonedimethane. *Surf. Sci.* **1998**, *419*, 12–23.
74. Torrente, I. F.; Franke, K. J.; Pascual, J. I. Structure and Electronic Configuration of Tetracyanoquinodimethane Layers on a Au(111) Surface. *Int. J. Mass Spectrom.* **2008**, *277*, 269–273.
75. Tseng, T.-C.; Urban, C.; Wang, Y.; Otero, R.; Tait, S. L.; Alcami, M.; Ecija, D.; Trelka, M.; Gallego, J. M.; Lin, N.; *et al.* Charge-Transfer-Induced Structural Rearrangements at Both Sides of Organic/Metal Interfaces. *Nat. Chem.* **2010**, *2*, 374–379.
76. Tseng, T.-C.; Abdurakhmanova, N.; Stepanow, S.; Kern, K. Hierarchical Assembly and Reticulation of Two-Dimensional Mn- and Ni-Tcnqx (X = 1, 2, 4) Coordination Structures on a Metal Surface. *J. Phys. Chem. C* **2011**, *115*, 10211–10217.
77. Schlickum, U.; Decker, R.; Klappenberger, F.; Zoppellaro, G.; Klyatskaya, S.; Auwärter, W.; Neppl, S.; Kern, K.; Brune, H.; Ruben, M.; *et al.* Chiral Kagomé Lattice from Simple Ditopic Molecular Bricks. *J. Am. Chem. Soc.* **2008**, *130*, 11778–11782.
78. Jävinen, P.; Hämäläinen, S. K.; Banerjee, K.; Häkkinen, P.; Ijäs, M.; Harju, A.; Liljeroth, P. Molecular Self-Assembly on Graphene on SiO_2 and h-Bn Substrates. *Nano Lett.* **2013**, *13*, 3199.
79. Torrente, I. F.; Franke, K. J.; Pascual, J. I. Spectroscopy of C60 Single Molecules: The Role of Screening on Energy Level Alignment. *J. Phys.: Condens. Matter.* **2008**, *20*, 184001.
80. Schiller, F.; Ruiz-Oses, M.; Ortega, J. E.; Segovia, P.; Martinez-Blanco, J.; Doyle, B. P.; Perez-Dieste, V.; Lobo, J.; Neel, N.; Berndt, R.; *et al.* Electronic Structure of C60 on Au(887). *J. Chem. Phys.* **2006**, *125*, 144719-1–144719-6.
81. Schulz, F.; Drost, R.; Hämäläinen, S. K.; Liljeroth, P. Templated Self-Assembly and Local Doping of Molecules on Epitaxial Hexagonal Boron Nitride. *ACS Nano* **2013**, 10.1021/nn404840h.
82. Nagashima, A.; Tejima, N.; Gamou, Y.; Kawai, T.; Oshima, C. Electronic Dispersion Relations of Monolayer Hexagonal Boron Nitride Formed on the Ni(111) Surface. *Phys. Rev. B* **1995**, *51*, 4606–4613.
83. Horcas, I.; Fernández, R.; Rodríguez, J. M.; Colchero, J.; Gómez-Herrero, J.; Baró, A. M. Wsxm: A Software for Scanning Probe Microscopy and a Tool for Nanotechnology. *Rev. Sci. Instrum.* **2007**, *78*, 013705.
84. CP2K developers group under the terms of the GNU General Public Licence.
85. VandeVondele, J.; Hutter, J. Gaussian Basis Sets for Accurate Calculations on Molecular Systems in Gas and Condensed Phases. *J. Chem. Phys.* **2007**, *127*, 114105.
86. Zhang, Y.; Yang, W. Comment on "Generalized Gradient Approximation Made Simple". *Phys. Rev. Lett.* **1998**, *80*, 890–890.
87. Grimme, S.; Ehrlich, S.; Goerigk, L. Effect of the Damping Function in Dispersion Corrected Density Functional Theory. *J. Comput. Chem.* **2011**, *32*, 1456–1465.
88. Childs, H.; Brugger, E.; Bonnell, K.; Meredith, J.; Miller, M.; Whitlock, B.; Max, N. A Contract Based System for Large Data Visualization. In *Visualization, 2005. VIS 05. IEEE*; IEEE: Piscataway, NJ, 2005; pp 191−198.